Astronomy & Astrophysics manuscript no. ForarXiv February 9, 2012
(DOI: will be inserted by hand later)

arXiv:1202.1086v2 [astro-ph.EP] 8 Feb 2012

The orbit of 2010 TK7. Possible regions of stability for other Earth Trojan asteroids

R. Dvorak[1], C. Lhotka[2], L. Zhou[3]

[1] Universitätssternwarte Wien, Türkenschanzstr. 17, A-1180 Wien, Austria,
[2] Départment de Mathématique (naXys), Rempart de la Vierge, 8, B-5000 Namur, Belgium,
[3] Department of Astronomy & Key Laboratory of Modern Astronomy and Astrophysics in Ministry of Education, Nanjing University, Nanjing 210093, China

Received; accepted

Abstract. Recently the first Earth Trojan has been observed (Mainzer et al., ApJ 731) and found to be on an interesting orbit close to the Lagrange point L4 (Connors et al., Nature 475). In the present study we therefore perform a detailed investigation on the stability of its orbit and moreover extend the study to give an idea of the probability to find additional Earth–Trojans. Our results are derived using different approaches: a) we derive an analytical mapping in the spatial elliptic restricted three–body problem to find the phase space structure of the dynamical problem. We explore the stability of the asteroid in the context of the phase space geometry, including the indirect influence of the additional planets of our Solar system. b) We use precise numerical methods to integrate the orbit forward and backward in time in different dynamical models. Based on a set of 400 clone orbits we derive the probability of capture and escape of the Earth Trojan asteroids 2010 TK7. c) To this end we perform an extensive numerical investigation of the stability region of the Earth's Lagrangian points. We present a detailed parameter study in the regime of possible stable tadpole and horseshoe orbits of additional Earth-Trojans, i.e. with respect to the semi-major axes and inclinations of thousands of fictitious Trojans. All three approaches underline that the Earth Trojan asteroid 2010 TK7 finds himself in an unstable region on the edge of a stable zone; additional Earth-Trojan asteroids may be found in this regime of stability.

1. Introduction

The giant planets Jupiter and Neptune are known to host Trojan asteroids, and also Mars (Bowell et al. 1990) is hosting several co-orbiting asteroids. These kind of bodies move in the same orbit as the planets, but around 60° ahead or 60° behind the planet close to the so-called Lagrange points L_4 or L_5 (see Fig. 1). It was a great surprise when quite recently the first Earth Trojan 2010 TK_7 was discovered (Mainzer et al. 2011). Although many studies have shown the principal possibility of their existence until this event all attempts of finding one were unsuccessful. Another small asteroid in the 1:1 mean motion resonance (MMR) with the Earth was found earlier in 1986, by Duncan Waldron and this asteroid (3753 Cruithne) was later identified as a celestial body in a horseshoe orbit around both equilateral Lagrange points of the Earth being thus not a 'real' Trojan in the sense of its original definition (the same is true for the recently found asteroid 2010 SO_{16}).

Many theoretical studies exist to establish the stability of the Lagrange points in simplified models, i.e. the works of (Rabe 1967; Bien & Schubart 1984; Lhotka et al. 2008; Érdi et al. 2009), beyond many others. Ever since extensive numerical studies have been undertaken in finding the extension of the stability regions around the equilibrium points for the planets, e.g. in (Schwarz et al. 2004; Dvorak & Schwarz 2005; Robutel et al. 2005; Freistetter 2006; Dvorak et al. 2007). Especially important results are due to the work of (Mikkola & Innanen 1992; Tabachnik & Evans 2000; Brasser & Letho 2002) and (Scholl & Marzari 2004). In (Mikkola & Innanen 1992) and (Zhang & Innanen 1995) the authors found that Venus, Earth and Mars can host co-orbital asteroids up to 10 Myrs. According to the investigation of (Tabachnik & Evans 2000) Earth's Trojans are on stable orbits when their inclinations are relatively low ($i < 16°$); a second stability window exists according to them for $16° < i < 24°$.

Morais & Morbidelli (2002) studied the orbital distribution of the near-Earth asteroids (NEAs) that experience the episode of being in the 1:1 MMR with the Earth. In a most recent study (Schwarz & Dvorak 2011) the possibility of captures of asteroids by the terrestrial planets into the 1:1 MMR was investigated and many temporary captures including jumping Trojans (Tsiganis et al. 2000) were found; as we will see also 2010 TK_7 has such an interesting captured orbit.

In our investigations – initiated by the finding of 2010 TK_7 – we concentrate on Earth Trojans. Three different ap-

Send offprint requests to: L. Zhou, e-mail: zhouly@nju.edu.cn, clhotka@fundp.ac.be, dvorak@astro.univie.ac.at, (authorlist in alphabetical order)

proaches should clarify the stability problem of these asteroids: in Chapter 2 we perform analytical studies in a simplified model, valid on short time scales. We investigate the phase phase structure and the influence of additional perturbations in the simplified model. In Chapter 3 we study in great detail the actual orbit of 2010 TK$_7$ together with 400 clone orbits to obtain a better statistics to state the probability of capture and escape of this Trojan asteroid. To this end we perform in Chapter 4 an extensive numerical investigation of the parameter space relevant to determine the stable and unstable regions close to the equilibrium point L_4 [1] and show the interplay between secular resonances and the stability of motion. The summary and conclusions of the present study are found in Section 5.

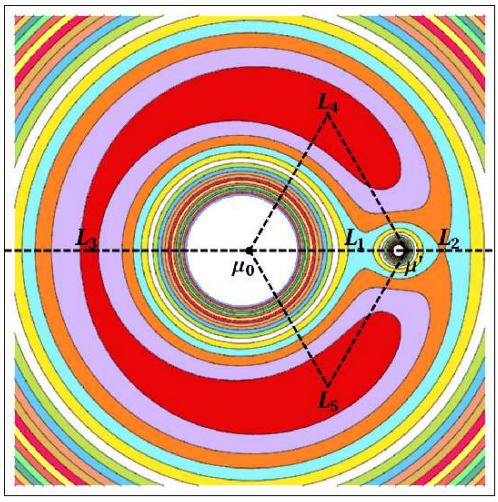


Fig. 1. Geometry of the circular restricted three–body problem in a rotating coordinate system: mass of the Sun μ_0 and the Earth μ'; the unstable equilibria $L_{1,2,3}$ are located on the x-axis; the stable points L_4 and L_5 are found 60° ahead and behind the primary mass μ'. The color code defines the areas of the equipotential. In the elliptic problem the rotating coordinate system has to replaced by a non uniformly rotating and pulsating reference frame.

2. A symplectic mapping model

The Hamiltonian describing the motion of 2010 TK$_7$ in the spatial elliptic restricted three–body problem (Sun-Earth-asteroid) takes the form:

$$H = H_{\rm Kep} + T + \mu' R(a, e, i, \omega, \Omega, M, M'; p') \qquad (1)$$

where H_{Kep} denotes the Keplerian part, the function $\mu' R$ is the perturbation due to the Earth with mass μ' and the variable T is the action conjugated to time (assuming, that the mean motion n' of the Earth is equal to one). Moreover, $a, e, i, \omega, \Omega, M$ are the semi-major axis, the eccentricity, the inclination, the perihelion, the longitude of the ascending node and the mean anomaly of the asteroid, respectively, while M' denotes the mean anomaly of the Earth.

[1] both Lagrange points have in principal the same dynamical behaviour as we know from earlier studies e.g. (Nesvorny & Vokrouhlický 2009; Zhou et al. 2009)

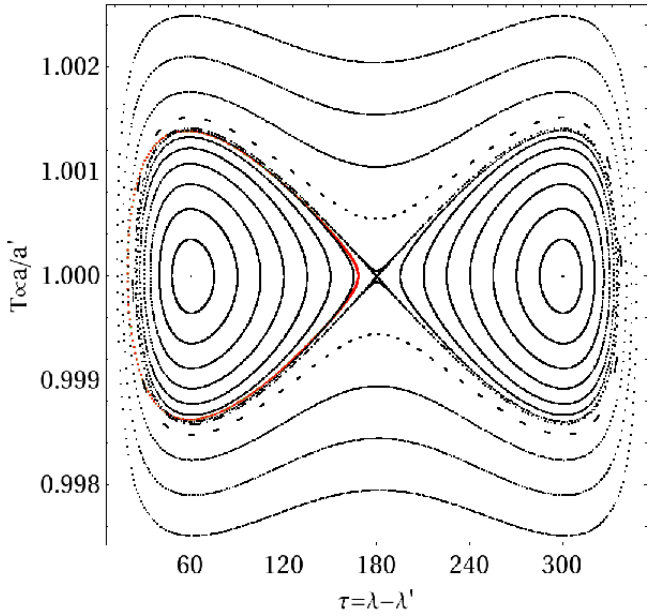


Fig. 2. Phase portrait - projected to the (τ, T)-plane. The Earth is located at $(0, 1)$, the fixed points L_4, L_3, L_5 (corresponding to the equilibria of the averaged system) are situated at $(60°, 1)$, $(180°, 1)$ and $(300°, 1)$, respectively. The projection of the mean orbit of the asteroid 2010 TK$_7$ for ±6000 years is shown in red.

In contrast to the classical expansion techniques of the perturbing function R we do not replace the remaining orbital parameters of the Earth $p' = (a', e', i', \omega', \Omega')$ with their numerical values but rather keep them as free parameters in the ongoing calculations. The simple reason for that is to be able to investigate their influence on the dynamics of the massless asteroid with time, i.e. to see their influence on the phase space geometry, later on. For the mapping approach we set the system of constants (gravitational constant G and total mass of the system) equal unity such that $G(\mu_0 + \mu') = 1$ which also implies that a' as well as a are close to unity and in these dimensionless units one revolution period of the Earth takes $P = 2\pi$. Furthermore, we use as action-angle variables the modified Delaunay variables which are defined in terms of the classical Delaunay variables by:

$$l = M,\ g = \omega,\ h = \Omega$$
$$L = \sqrt{a},\ G = L\sqrt{1-e^2},\ H = G\cos(i)$$

as

$$\lambda_1 = l + g + h,\ \lambda_2 = -g - h,\ \lambda_3 = -h$$
$$\Lambda_1 = L,\ \Lambda_2 = L - G,\ \Lambda_3 = G - H$$

(and similar for the primed variables of the Earth). In this setting, the Hamiltonian (1) becomes:

$$H = -\frac{1}{2{\Lambda_2}^2} + T + \mu' R(\lambda, \Lambda, \lambda_1', q') \qquad (2)$$

where we used the short-hand notation $\lambda = (\lambda_1, \lambda_2, \lambda_3)$ and $\Lambda = (\Lambda_1, \Lambda_2, \Lambda_3)$. In addition we abbreviate the parameter vector $q' = \left(\lambda_2', \lambda_3', \Lambda_1', \Lambda_2', \Lambda_3'\right)$ to define the vector of modified

Delaunay variables for the Earth. Next, we implement a symplectic change of coordinates and momenta suitable to describe the motion of the asteroid close to the 1 : 1 MMR. We define the resonant angle and conjugated momenta as:

$$\tau = \lambda_1 - \lambda_1', \; T = \Lambda_1 \tag{3}$$

while the other variables transform by the identity:

$$\lambda_2 = \varphi, \; \lambda_3 = \theta, \; \Lambda_2 = \Phi, \; \Lambda_3 = \Theta$$

and $T' = \Lambda_1 - \Lambda_1'$. We replace λ_1 in (2) according to (3) and implement the standard averaging procedure over the fast angle λ' via the formula:

$$\tilde{H} = -\frac{1}{2T^2} + \frac{1}{P}\int_0^P \mu' R\,(\lambda, \Lambda, \lambda_1'; q')\,\mathrm{d}\lambda' \;, \tag{4}$$

with $P = 2\pi$, to get the averaged Hamiltonian function of the form $\tilde{H} = \tilde{H}(\psi, \Psi; q')$ with $\psi = (\tau, \varphi, \theta)$ and $\Psi = (T, \Phi, \Theta)$. Our aim is to construct a symplectic mapping which transforms the state vector $(\psi_k, \Psi_k) \equiv (\tau_k, \varphi_k, \theta_k, T_k, \Phi_k, \Theta_k)$ at discrete times k (multiples of P) to the state vector (ψ_{k+1}, Ψ_{k+1}) at times $k + 1$. For this reason we define the generating function

$$W_{q'} = W_{q'}\,(\tau_k, \varphi_k, \theta_k, T_{k+1}, \Phi_{k+1}, \Theta_{k+1}; q') = \\ \psi_k \cdot J_{k+1} + 2\pi\tilde{H}\,(\psi_k, J_{k+1}; q') \;,$$

where the symbol $\cdot$ is the dot product. As it has been shown and already used in (Hadjidemetriou 1992; Hadjidemetriou 1999; Hadjidemetriou & Voyatzis 2000) or (Ferraz-Mello 1997) the generating function defines a mapping of the form:

$$\tau_{k+1} = \frac{\partial W_{q'}}{\partial T_{k+1}}, \;\; \varphi_{k+1} = \frac{\partial W_{q'}}{\partial \Phi_{k+1}}, \;\; \theta_{k+1} = \frac{\partial W_{q'}}{\partial \Theta_{k+1}}, \\ T_k = \frac{\partial W_{q'}}{\partial \tau_k}, \;\; \Phi_k = \frac{\partial W_{q'}}{\partial \varphi_k}, \;\; \Theta_k = \frac{\partial W_{q'}}{\partial \theta_k} \;\; . \tag{5}$$

System (5) defines a symplectic change of coordinates on the Poincaré surface of section obtained by the averaged system defined by (4). The set of variables (Ψ, ψ) is related to the mean orbital elements of the asteroid 2010 TK$_7$ via another generating function (not derived here) which defines the averaging process given in (4). The system (5) therefore describes the evolution of the mean orbital elements of the asteroid at discrete times $t = k \cdot P$. Note, that the system is implicit to preserve the Hamiltonian structure of the original problem. For given initial conditions $(\psi_{k=0}, \Psi_{k=0})$ it can either be iterated by solving the system of difference equations implicitly for (Ψ_{k+1}, ψ_{k+1}) or by more sophisticated procedures as described e.g. in (Lhotka 2009).

A typical projection of the phase portrait to the (τ, T)-plane is shown in Fig. 2. The lines in black were obtained by varying τ within $(0°, 360°)$ along $T = 1$. The plot also shows the mean orbit of 2010 TK$_7$ in red. It has to be compared with Figure 2 of (Connors et al. 2011): while the authors derive the red curve by numerical averaging, the averaged orbit of the present approach is based on Eq. (5).

As it is well-known, e.g. (Morais & Morbidelli 2002; Brasser & Letho 2002; Scholl et al. 2005), the influence of the other Solar system bodies, i.e. the direct influence of the major planets, affects the motion of the asteroids on long time scales. The mapping does not take into account these direct effects. Thus, the mean orbit as shown in Fig. 2 can only been seen as a first approximative solution of the problem. Moreover, the simulations were done using low order expansions of the perturbing function, since we wanted to keep the dependency of the model on the orbital parameters of the Earth. The resulting mapping model is therefore only valid within a good convergence regime of the Fourier-Taylor series expansions used to approximate R in (1). In addition, since the orbital parameters of the asteroid 2010 TK$_7$ may reach high values (as found from numerical simulations) the error of the approximation of the series expansions may exceed the cumulative effect of the perturbation effects due to the Solar system and may also change the picture dramatically on longer time scales. An estimate of the error terms and higher order series expansions together with their influence on the long term dynamics of the asteroid 2010 TK$_7$ is currently under investigation.

3. The orbit of 2010 TK$_7$

The Earth Trojan 2010 TK$_7$ fundamentally is a NEA, and its orbital elements (listed in Table 1) can be found also on the AstDyS (*Asteroids - Dynamic Site*) website [2]. At first glance, this object has a large eccentricity (~ 0.19) and it is reasonable to suspect that it's on a unstable orbit. To check the orbital stability of this object, we perform numerical simulations of the orbit.

We adopt two dynamical models in our simulations. Both models contain the Sun and 8 planets from Mercury to Neptune. They differ from each other by different settings of the Earth-Moon system. In one model, the Earth-Moon system is simply treated as one mass point with the combined mass of the Earth and the Moon at the barycenter of the system. And in the other model, the Earth and the Moon are regarded as two separated objects as in reality. Hereafter we denote the former by EMB model and the latter by E+M model for short. By comparing these two models, we may testify the reliability of the model adopted later in this paper and also by (Connors et al. 2011) in their numerical simulations.

Considering the uncertainties in observation and orbital determination, it is necessary to study clone orbits within the error bars. Beside the nominal orbit, 400 clone orbits are generated using the covariance matrix given by the AstDyS website. As listed in Table 1, the errors are very small, therefore the initial conditions of the clone orbits are very close to the nominal orbit as shown in Fig. 3. We show here the distribution of a, e, i and Ω, the other two elements M, ω not illustrated here have similar distributions according to the corresponding uncertainties listed in Table 1.

Starting from the initial conditions generated in the above way, we integrate their orbits up to 1 million years (Myr) in both directions (forward to the future and backward to the past). We used the integrator package *Mercury6* (Chambers 1999) and verified some results using the Lie-integrator (Hanslmeier & Dvorak 1984). The comparison be-

[2] http://hamilton.dm.unipi.it

Table 1. The Keplerian elements of 2010 TK_7 given at epoch JD2455800.5. The elements and $1-\sigma$ variations are from the AstDyS (see text). The covariance matrix is also taken from the same website.

	Value	1-σ variation	Unit
a	1.00037	2.546×10^{-7}	AU
e	0.190818	9.057×10^{-7}	
i	20.88	7.274×10^{-5}	deg.
Ω	96.539	1.842×10^{-4}	deg.
ω	45.846	2.309×10^{-4}	deg.
M	217.329	1.848×10^{-4}	deg.

tween the results from different integrators shows that the results are consistent with each other.

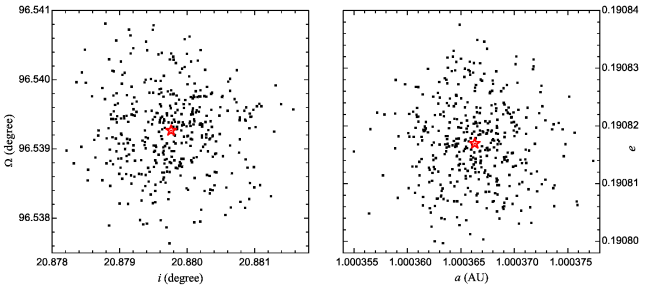


Fig. 3. The initial conditions of clone orbits. Dots are for 400 clones, and the nominal orbit is indicated by the red star. We show here in two panels only the inclination, ascending node, semimajor axis and eccentricity.

For an asteroid on a Trojan-like orbit, the critical angle (resonant angle) is the difference between the mean longitudes of the asteroid λ and the corresponding host planet (here it's the Earth-Moon system) λ', like the τ in Eq. (3). In the EMB model the resonant angle is $\lambda-\lambda_{\rm EMB}$, while in the E+M model we calculate the position and velocity of the barycenter of the Earth-Moon system from the orbital elements of the Earth and the Moon, and then compute the resonant angle in the same way as in the EMB model. When the resonant angle $\lambda-\lambda'=\lambda-\lambda_{\rm EMB}$ librates around 60°, i.e. $0^\circ<\lambda-\lambda'<180^\circ$, the asteroid is said to be an L_4 Trojan, when it librates around -60° or 300°, i.e. $180^\circ<\lambda-\lambda'<360^\circ$ it is an L_5 Trojan, when the asteroid librates with an amplitude larger than 180° it is on a horseshoe orbit, and finally when $\lambda-\lambda'$ circulates the asteroid leaves the Trojan-like orbit.

In Fig. 4, we illustrate the temporal evolution of the nominal orbit in the E+M model. The first impression obtained from its behaviour may be that it's a temporal Earth Trojan, i.e. judging from the resonant angle it was not an Earth Trojan 0.055 Myr before and it will not stay on a Trojan-like orbit after 0.37 Myr. The period of its being an L_4 Trojan is even much shorter, less than 2,000 years in the past and less than 17,000 years in the future (as partly shown in Fig. 5). During the period of being a Trojan, the semimajor axis a shows regular variations librating around 1.0 AU with a small amplitude, however, the variations of eccentricity e and inclination i reveal the chaotic character of the motion, as shown in Fig. 4.

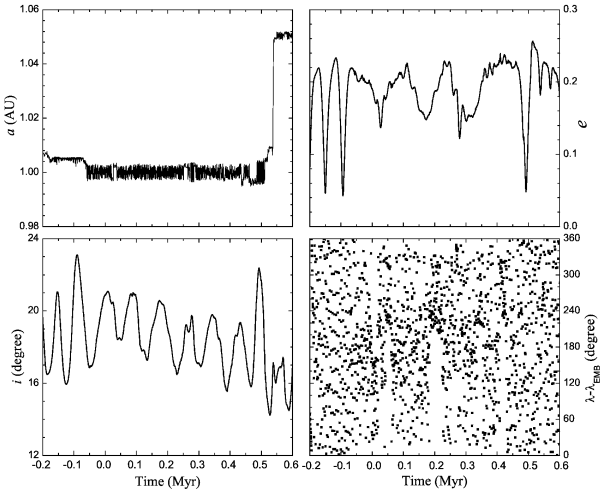


Fig. 4. The temporal evolution of the nominal orbit in 1 million years, both forward and backward. In four panels we show the evolutions of the semimajor axis (upper left), eccentricity (upper right), inclination (lower left) and the resonant angle (lower right).

The chaotic character of the motion implies not only a sensitive dependence on the initial conditions but also a sensitive dependence on the dynamical model. To compare the motions in two models, i.e. the EMB model and E+M model, we show as an example in Fig. 5 the evolution of the resonant angle of the nominal orbit in both models. Around the starting point, two curves representing the motions in two models are almost the same so that they overlap each other exactly. But the difference between them becomes distinguishable only after about 2,000 years in both directions. This difference on one hand arises from the different settings of the models, on the other hand, it is due to the chaotic character of the motion. In this sense, it is impossible to draw any convincible conclusion about these two dynamical models on long time scales by comparing just the motions of an individual orbit in two models. So we turn to analyze statistically the four hundred clone orbits below.

As we mentioned above, 400 clone orbits are calculated in both models and in both directions of time. At starting moment $t=0$ these clones are around the L_4 Lagrange point as the asteroid 2010 TK_7, but in the evolution, the objects may jump from the L_4 region to L_5 region, or they may move from tadpole orbit to horseshoe orbit, and even, they may escape from the Trojan-like orbit (the 1:1 MMR). To examine the motion, we check the resonant angle $\lambda-\lambda_{\rm EMB}$ at each step during our simulations. When $\lambda-\lambda_{\rm EMB}$ for the first time is larger than 180°, the object is regarded as leaving the L_4 region, and we denote the time at this moment as t_1. When $\lambda-\lambda_{\rm EMB}$ reaches for the first time 360°, the object escapes the 1:1 MMR, and we denote this moment as t_2.

The t_1 and t_2 of 400 clone orbits are summarized in Fig. 6 and Fig. 7. For t_1, most of the clones will leave the L_4 region in

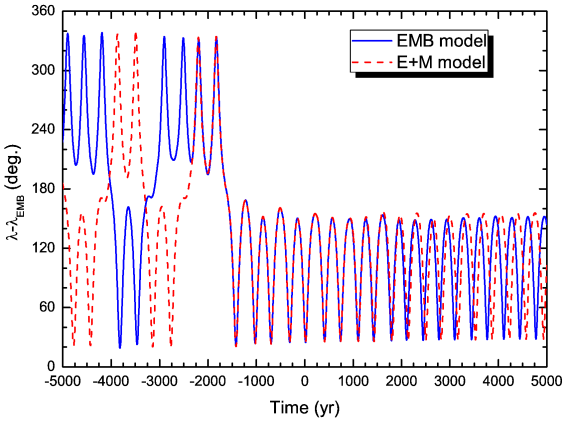


Fig. 5. The resonant angle of the nominal orbit in two models. The difference between them is distinguishable very soon (~ 2000 years) mainly due to the chaotic character of the motion (see discussion in text).

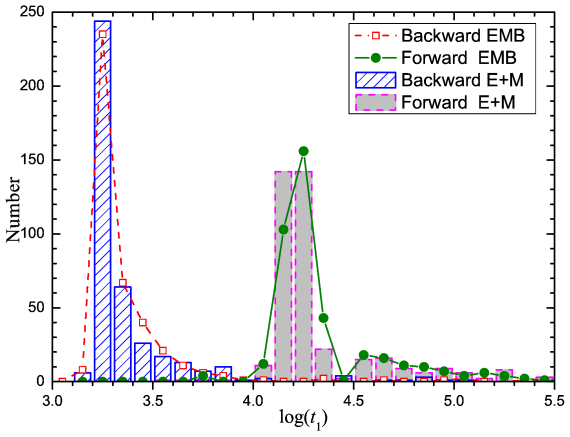


Fig. 6. The distribution of the time when clone orbits leave from current L_4 region. The escape time from the tadpole region is given in years in logarithm scale.

about 1.5×10^4 years in future, while the backward integrations indicate that the clones "entered" the L_4 region in about 1.8×10^3 years ago (Fig. 6).

In the backward integrations, the earliest escape from the L_4 region happens at $t\sim1440$ years both in the E+M and EMB models. But there are only a few such orbits. Most of them escape in the time range between $t\sim1680$ and $t\sim1820$ years which causes the peak centered at $\log(t_1)=3.25$ in Fig. 6. In fact, from Fig. 5, we may derive the libration period of the resonant angle is around 350 years[3], and we also note that the shift of the orbit from L_4 to L_5 region happens when the resonant angle reaches the maximum in a libration period. The libration period and amplitude must be tuned by other periodic effects (e.g. secular resonances). After a number of complete periods of evolution, the resonant angles of some clone orbits reach their maxima, and they do not librate back but escape from there towards the neighbourhood of L_5. After another complete libration period, many more clone orbits escape in the same way as before. That's why the escapes from the L_4 region seem to happen more or less suddenly (at $t\sim1440+350=1790\approx10^{3.25}$ years). All clone orbits are in a tiny region confined by the error bars, so that they suffer nearly the same dynamical effects in a short timespan. For those clones staying in the region longer, they spread in the phase space and thus suffer different dynamical effects and consequently their escape times diverge.

The distributions of t_1 for the EMB model and the E+M model in Fig. 6 match each other very well, therefore we may draw another conclusion here that the difference between these two dynamical models is ignorable, or in other words, the simplified EMB model is a reasonable and reliable model for investigating the Earth Trojans' long term dynamics. Particularly, we would like to note that the asteroid 2010 TK$_7$ and the clones all have very large libration amplitudes around the L_4 and/or L_5 point (see for example Fig. 5), i.e. they may approach to the Earth-Moon system (mean longitude difference between them may be less than 20°). But in fact, even when an Earth Trojan approaches the Earth to within 10° apart in mean longitude, the distance between the asteroid and the Earth is about 0.18 AU, which is still about 70 times larger than the distance between the Earth and the Moon. Taking into account the inclination of the Earth Trojan's orbit, the distance between the Trojan and the Earth is even larger.

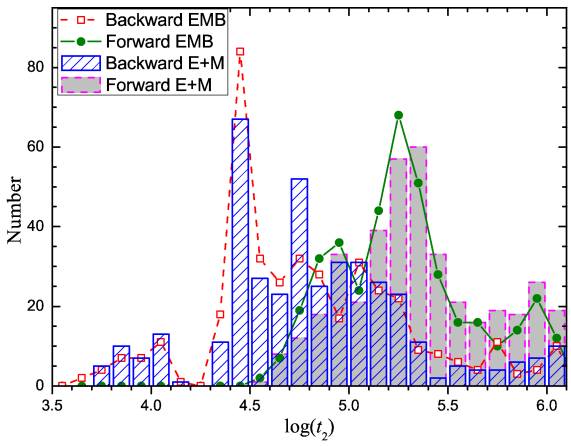


Fig. 7. The distribution of the time when clone orbits escape from the 1:1 MMR, both in forward and backward integrations. The escape time is given in years in logarithm scale.

As for t_2 distribution in Fig. 7, we see the peak of escaping time in the backward integrations locates at $\sim3.0\times10^4$ years. As we mentioned above, the Earth Trojan 2010 TK$_7$ should be a temporal Trojan. The capture of this asteroid onto the 1:1 MMR with the Earth happened most probably 30,000 years ago. In the forward integrations, most of clones will escape from the MMR around 2.0×10^5 years after. The total lifetime of this asteroid in the 1:1 MMR is less than 0.25 Myr. And again, the two models E+M and EMB give nearly the same distributions.

In our calculations, the episode of clones being L_4 Earth Trojans lasts typically a little less than ~ 17,000 years. As for

[3] Due to the large libration amplitude, this value is nearly 50 percent larger than the synodic period of a tadpole orbit which can be estimated using the formula $(27\mu/4)^{-1/2}$ (Murray & Dermott 1999). For an Earth Trojan, the mass ratio $\mu=3.04\times10^{-6}$ and the period is ~ 220 years.

the lifetime of clones staying in the 1:1 MMR, there are 10 clones surviving 1 Myr in the backward integrations in both models, while for the forward integrations, 12 in the EMB model and 19 in the E+M model stay in the MMR till the end of integrations. But none of the clones survives in both temporal directions. In one word, less than 5 percent of clones stay in the MMR up to 1 Myr. Morais & Morbidelli (2002) calculated the probability of a NEA being captured into the 1:1 MMR ("coorbital orbit" in their paper), and they found that each episode of a NEA being coorbital on average is 25,000 years and none lasts longer than 1 Myr. Our result does not conflict with their conclusion, because our calculations are for the individual asteroid 2010 TK_7, and its eccentricity (~ 0.2) is smaller than the typical eccentricity in their samples (most of them have $e > 0.28$).

Some fluctuations in the distribution of t_1 and t_2 (by "fluctuation" we mean more peaks deviated from a trivial normal distribution) can be found in both models in Fig. 6 and Fig. 7. In these figures, the time is given in logarithm to include a wide time range. If we plot the time linearly, these fluctuations show some periodic character, implying that some periodic mechanisms (e.g. secular resonances) are affecting the libration amplitudes. However to depict a secular resonance map is a long story, we would like leave it to a separate paper but show first results in Section 4.3.

4. Determination of the stable regions

As was pointed out in the previous sections the orbit of 2010 TK_7 is not very stable. The goal of this part of our investigation is to determine the largeness of the stable regions arou the stable equilibrium points. This can be done in a real tic dynamical model only with the aid of numerical integ tions where many fictitious Trojans are checked concerni the stability of their orbits. The dynamical model used was 'truncated' planetary system with the planets Venus to Satu (Ve2Sa). The simple reason for not taking into account all t planets is that it would at least require four times longer CI times on our computers. It is mainly due to the orbit of the i nermost planet Mercury which demands for a step size of o quarter of the one of Venus[4]. Test computation for selected s ble and unstable orbits showed that the qualitative behavc of such orbits is not a different one and consequently also t largeness of the stable region can be regarded as the 'real' or It means that the gravitational perturbation of Mercury on Trojan for this study is neglectable. The Moon was not e plicitly integrated but the barycenter Earth Moon with the r spective masses was taken as one body. As has been shown Chapter 3 there are only very small differences when one i tegrates the Trojan orbits in these models, on long time scales. On the contrary Jupiter's direct perturbation on an Earth Trojan is very large and cannot be neglected especially for large librations which bring the Trojan close to the Lagrange point L_3.

The integration method was the Lie-series method which we used already quite often in similar investigations (e.g. for Neptune (Zhou et al. 2009; Zhou et al. 2011) and recently also Uranus' Trojans (Dvorak et al. 2010)). This method is based on a work by (Hanslmeier & Dvorak 1984; Delva 1984) and (Lichtenegger 1984) and was slightly modified for our problem (see also (Eggl & Dvorak 2010)). It has an automatic step-size control and turned out to be fast and precise.

The initial conditions were chosen in the following way: for the fictitious Trojans the orbital elements M, Ω, e were set to the one of the Earth. The perihelion was always $\omega_{Earth} + 60°$ [5], the semimajor axes for the Trojan was set to slightly smaller and larger values to cover the stable region (along the connecting line between Sun and the Lagrange point). We started with integrations in the plane of the orbit of the Earth and changed in additional runs the inclinations up to $i = 60°$.

As to distinguish between stable and unstable orbits we used different indicators: the most straightforward was to check the eccentricity of the object because there turned out to be a sharp cut for $e > 0.3$: any orbit which achieved this value during the integration left the area around the Lagrange point (checked by its distance to this point). In another test we computed directly the escape times and finally we also computed the libration width of the Trojan which is a well established check of stability for a Trojan. The length of integration was thoroughly chosen; although we had a computer grid available the main computations covered only 10^7 years but some tests has been undertaken up to 10^8 years.

4.1. The stable regions for different time scales

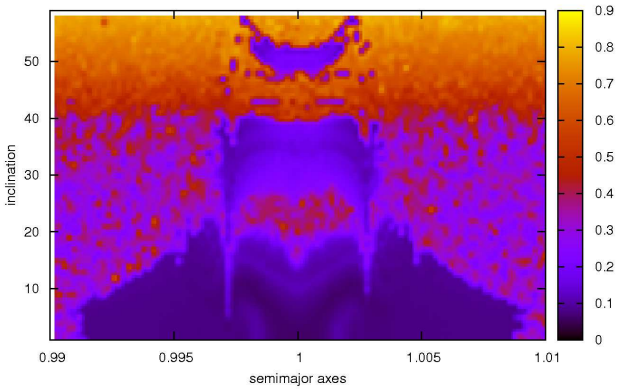


Fig. 8. Stability diagram using e_{max} for the window between $i < 60$ (y-axes) for different initial semimajor axes (x-axes) of the fictitious Trojans; the color stands for the maximum eccentricity during the integration of 10^6 years.

The stability diagram for a cut through the Lagrange point L_4 is shown in Fig. 8 where we plotted the maximum eccen-

[4] The inclusion of Uranus and Neptune would not dramatically change this integration time

[5] which means that the position was the Lagrange point L_4

tricity of the orbits of 100 massless fictitious Trojans for d ferent values of the semimajor axes (x-axes) versus the inc nations of the Trojan (y-axes). One can see that for small i clinations the stable region extends in semimajor axes betwe $0.99 \leq a \leq 1.01$, then there is a decrease of the largeness the region visible up to about $i = 20°$. Inside this region tv finger-like slightly less stable regions are visible on both sid of the a V-shaped structure centered at $a = 1$ leading frc $15° \leq i \leq 20°$. Then an unstable strip follows to about $i = 2$ with some connection to a larger rectangular stable region w $0.997 \leq a \leq 1.003$ and $26° \leq i \leq 40°$. Stable symmet fingers inside this region are clearly visible and build a conti uation of the unstable fingers around $a \simeq 0.997$ and $a \simeq 1.0$ for the large stable area for $i < 20°$. For larger inclinatio on $i > 40°$ the unstable regions extends for all values of t semimajor axes with the exception of a small U-shaped stat window around $i = 50°$. Note that inside this unstable regi (red to yellow) sometimes small stable island seem to appe on both sides of the stable region $i < 40°$ which - after a long integration - disappear.

Concerning the structures visible in the figure mentioned above we note that similar ones have been discovered for the Trojan regions of the outer planets in the papers by (Michtchenko & Ferraz-Mello 2002) and (Nesvorný & Dones 2002) for larger eccentricities. In our paper we investigated the stability for larger inclinations; the different features inside stable regions for Earth Trojans are comparable to the ones found by (Zhou et al. 2009) for the Neptune Trojan region. The instabilities inside the stable region are caused by secular resonances – as it has been shown in detail for the Jupiter Trojans by (Robutel & Gabern 2006). In our article we just want to show – for the moment – the complicated structures. To make a detailed analysis concerning the resonances like in the paper by (Zhou et al. 2009) or even the former mentioned article by (Robutel & Gabern 2006) takes quite a long time; we started this work already.

In a next step we extended the integration to 10^7 years in the same dynamical model Ve2Sa. The region for small inclinations is still stable with the same extension in semimajor axes (Fig. 9). New features, unstable vertical strips, appear for different values of a and increasing values of the inclination. For $a \simeq 0.997$ and $a \simeq 1.003$ these regions were already visible as being less stable in the former plot (Fig. 8) for small inclinations. New unstable vertical fingers appear also for $a \sim 0.995$ and $a \sim 1.005$ and $10° < i < 16°$. A new characteristic is the appearance of unstable fingers for $a \sim 0.998$ and $a \sim 1.002$ with $i < 6°$. The V-shaped unstable region centered at $a = 1$ was already visible in Fig. 8 but the detailed structures become more clear using a longer integration time.

In the next Fig.10 the stable window for $28° < i < 40°$ was studied separately (also for 10^7 years). Again one can see that the most stable regions visible through the dark blue – indicating small e-max values – are close to the edges in a. These edges are quite irregular and some smaller unstable islands appear inside; the whole stable region is somewhat tattered. What we do not show here is the disappearance of the U-shaped island for $i \sim 50°$ for a longer integration time.

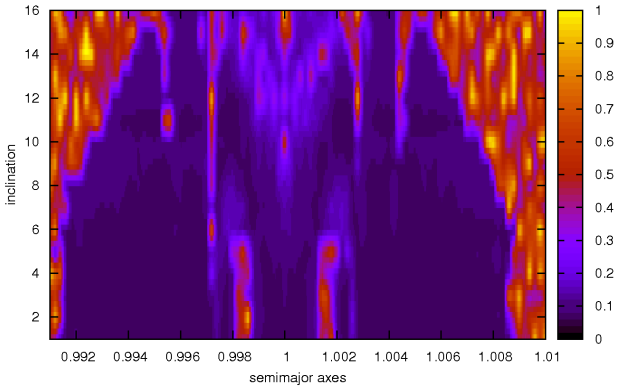


Fig. 9. Caption like for Fig. 10.

We note that we disagree, in some aspects, with the results given by (Tabachnik & Evans 2000) who claim that stable regions for Earth Trojans are possible for $24° < i < 34°$; the stable window we found is shifted outwards to larger inclinations. We also disagree with the later paper by (Brasser & Letho 2002) where they say that orbits with an inclination of $12° < i < 25°$ on are unstable. In the last work the authors quite nicely determine the secular frequencies involved leading to unstable motion. We already started additional computations where the determination of the resonances are undertaken, but their detailed analysis will be shown in a longer article (in preparation).

4.2. The libration amplitudes

To determine the libration width of the region we choose for the semimajor axes a grid of $0.995 \leq a \leq 1.005$ for 50 different fictitious bodies equally distributed in the mentioned interval where the inclination was set to values $0° \leq i \leq 56°$. The integration time was only 10^6 years for this study. The colors (from blue to yellow) indicate the amplitude of libration; we can see a well defined stable region in the range $0.997 \leq a \leq 1.003$ for inclinations $i \leq 19°$. This rectangular like region seems to contradict the results shown in Fig. 8, but a closer look shows – through the color of dark yellow – that the libration angle is in the order of 170°; thus on the edge we have horseshoe orbits which enclose both equilateral Lagrange points. An unstable strip then arises $20° \leq i \leq 24°$ where close to $a \sim 1.0005$ and $i \sim 21°$ the 2010 TK_7 is located. Then we see again a large almost rectangle like stable region $25° \leq i \leq 39°$ for the same range of a as the first stable region of tadpole orbits for only slightly inclined Trojan orbits. Note that the edges are sharp and no horseshoe orbits are located there. From $i = 40°$ no more stable orbits exist with the exception of a small stable

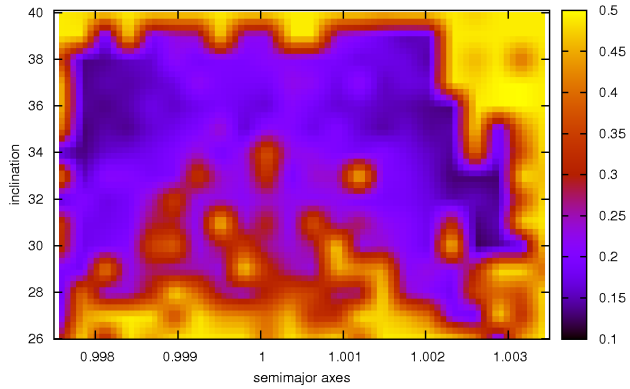


Fig. 10. Stability diagram using e_{max} for the window between $26 < i < 40$ (y-axes) for different initial semimajor axes of the fictitious Trojan; the color stands for the maximum eccentricity during the integration of 10^7 years.

window with tadpole orbits for $i \sim 50°$; these orbits will be unstable for longer integration time as indicated above.

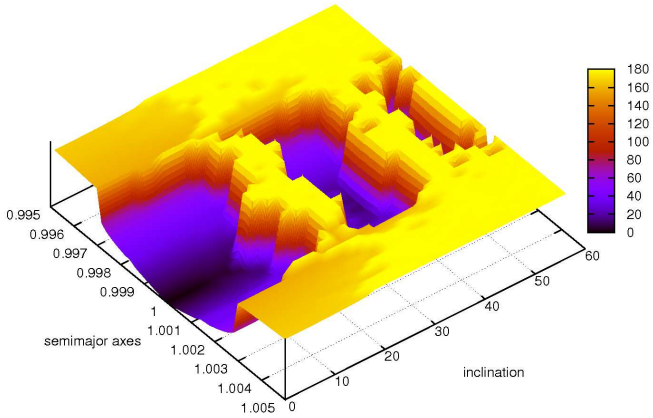


Fig. 11. Libration amplitudes – defined as half of the total libration angle – in the region close to L_4; the color stands for the largeness of the libration.

To show the different kinds of orbits we depict three different ones for an inclination of the Trojan's orbit $i = 1°$: a tadpole orbit deep inside the stable region (Fig. 12 upper graphs), a horseshoe orbit close to the border of stability (Fig. 12 middle graphs) and an escaping orbit outside the stable region after initially being in a horseshoe orbit (Fig. 12 lower graphs). On the left pictures of this figure the semimajor axes show a periodic change between a maximum and a minimum value close to the semimajor axis of the Earth for the tadpole and the horseshoe orbit. In the middle graph the typical behaviour for a body in a horseshoe orbit is shown which we can describe at the best in a rotating coordinate system (comp. Fig. 1): close to the turning point of the orbit the Trojan finds itself in the vicinity of the Earth, the semimajor axes is larger than the one of the Earth and then – when the libation angle changes from about 10° to 350° it reaches values smaller than a_{Earth}; now the Trojans is on the other side of the Earth. In Fig. 12 in the lowest graphs an unstable orbit is shown which – after leaving to be in a horseshoe orbit – is chaotic with librations between 0° to 360°.

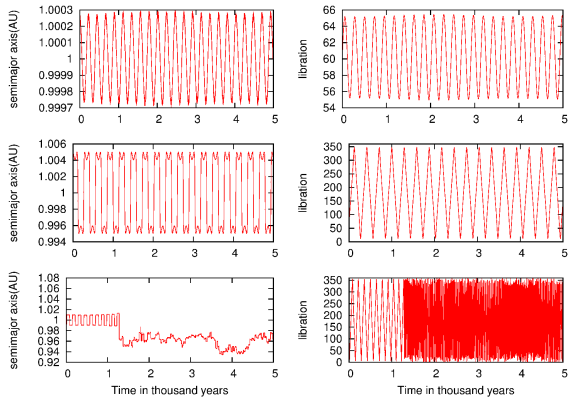


Fig. 12. The temporal evolution of three orbits: a tadpole (upper graphs) a horseshoe (middle graphs) and an escaping orbit (lower graphs) In six panels we show the evolutions of the semimajor axis (left graphs) and the libration angles (right graphs) during 5000 years.

4.3. Secular resonances

In this part we present our preliminary results about the secular resonances to understand the structure of the stability diagram (Fig. 8). A secular resonance happens when the precession rate of an object ($\dot{\varpi}$ or $\dot{\Omega}$) equals to one of the eigenfrequencies of the system (Murray & Dermott 1999). In a secular resonance, the eccentricity or the inclination shows long-term oscillations. The eigenfrequencies of the system can be calculated through a linear analysis (Brétagnon 1974) or can be numerically determined (Laskar 1990).

The reality is more complicated than the model adapted in the linear analysis. The secular perturbations among the planets modify the precession rates. Due to their large masses the ones of the big planets are almost constant; on the contrary, the precession rates of the inner planets are strongly influenced particularly by Jupiter and Saturn. In Fig. 13, we show the differences between Jupiter's perihelion longitude (ϖ_5, as usually denoted) and the ones of Venus (ϖ_2) and the Earth (ϖ_3) in our

simulations. Obviously, during the periods ~ 0.05 – 0.35 Myr and ~ 0.45–0.75 Myr, ϖ_2 and ϖ_3 have nearly the same precession rate as Jupiter. This makes the secular evolution of asteroids in this planetary system complicated, as we will see below.

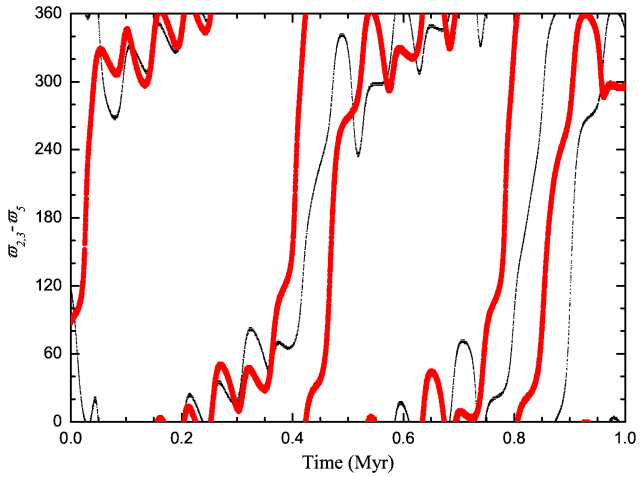


Fig. 13. The differences between perihelion longitudes of inner planets and of Jupiter. The abscissa is time and the ordinate is $\varpi_k - \varpi_5$, with $k = 2$ for Venus (thin black curve) and $k = 3$ for the Earth (thick red curve).

At high inclinations the Kozai resonance causes large coupled variations of the eccentricity and the inclination (Brasser et al. 2004), which finally results in instability. At low and moderate inclinations the secular resonances ν_3 and ν_4 were found to affect the Earth Trojans[6] (Morais 2001; Brasser & Letho 2002). We notice there are some disagreements in the locations of these secular resonances between different papers. To depict a detail resonance map we would like to leave it to a separate paper. Here we only illustrate the evolution of four typical orbits to show the effects of secular resonances that contribute to form the structures in the stability diagrams. In Fig. 8 these are the four orbits with semi-major axis $a = 0.9995$ AU and inclination $i = 10°, 22°, 35°, 42°$; the evolutions of the resonant angles are presented in Figs. 14 and 15, respectively. The signal of the eccentricities can be found in Fig. 16. Obviously, the orbits with $i = 10°$ and $i = 35°$ are in the stable windows, while the orbits with $i = 22°$ and $i = 42°$ are in the unstable gaps in Fig. 8.

Our preliminary calculations show that the most important secular resonances affecting the Earth Trojans are ν_2, ν_3, ν_4 and ν_5. According to the linear theory of secular perturbation, the averaged temporal variation of the eccentricity of a celestial body perturbed by a perturbing planet can be roughly approximated by

$$< \dot{e} >= C \sin(\Delta\varpi_i) = C \sin(\varpi - \varpi_i) \,, \qquad (6)$$

where C is a negative constant determined by the mass of the planet and the Laplace coefficients (Murray & Dermott 1999; Li et al. 2006), ϖ and ϖ_i are the perihelion longitudes of the celestial body and the planet, and $\Delta\varpi_i = \varpi - \varpi_i$ with $i = 1, ..., 5$. If $0° < \Delta\varpi_i < 180°$ then $< \dot{e} >$ is less zero and if $180° < \Delta\varpi_i < 360°$ then $< \dot{e} >$ is greater zero.

[6] A Trojan precesses at the rate of the eigenfrequency g_3 (or g_4), which is the precession rate of the Earth (or Mars), is in the ν_3 (or ν_4) secular resonance.

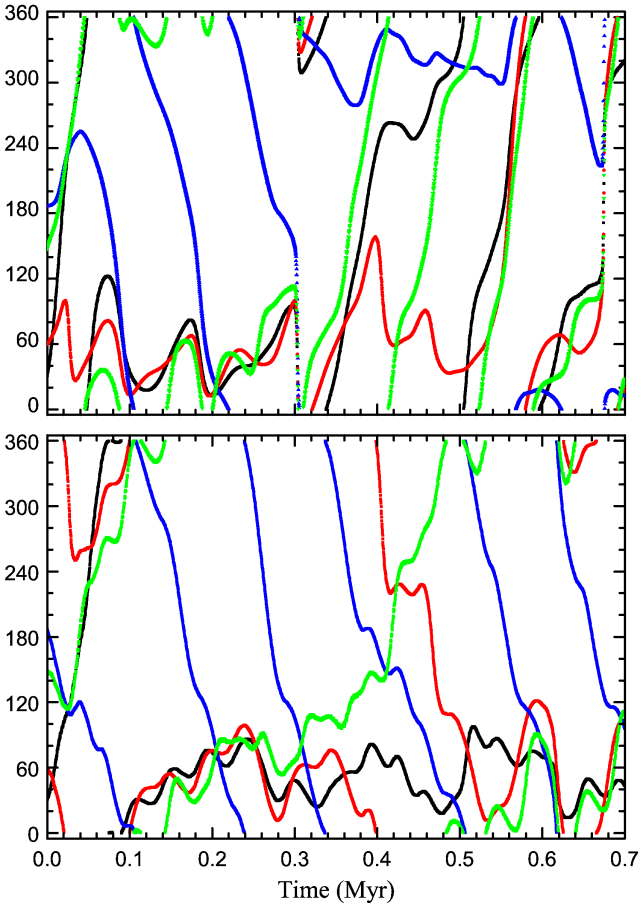


Fig. 14. The evolution of apsidal differences between the Trojans and the planets: $\Delta\varpi_2 = \varpi - \varpi_2$ (black), $\Delta\varpi_3 = \varpi - \varpi_3$ (red), $\Delta\varpi_4 = \varpi - \varpi_4$ (blue) and $\Delta\varpi_5 = \varpi - \varpi_5$ (green). The upper panel is for $i = 10°$ and the lower panel is for $i = 35°$.

For the orbit with $i = 10°$, from $t = 0.05$ Myr to 0.3 Myr the angles $\Delta\varpi_2$, $\Delta\varpi_3$ and $\Delta\varpi_5$ librate, all around values ~ 40° (see Fig. 14, upper panel). Such libration affects (but not excites, according to Eq. 6) the eccentricity of the Trojan. The overlap of these secular resonances introduces chaos to the motion, which can be seen in the irregular eccentricity evolution (black in Fig. 16). After $t = 0.3$ Myr the ν_2 and ν_5 vanishes as the corresponding resonant angles circulate, but $\Delta\varpi_4$ begins to librate around a value larger than 180°, i.e. ν_4 resonance appears. Although this ν_4 resonance may increase the eccentricity since $\Delta\varpi_4 > 180°$, this eccentricity pumping effect is offset by the ν_3 resonance, which is continuously present with the $\Delta\varpi_3 < 180°$.

Similar evolution happens for $i = 35°$ (see Fig. 14, lower panel). In this case, before $t = 0.1$ Myr however, ν_3 and ν_5 librate around high values, resulting in eccentricity excitation in this period (blue in Fig. 16). The ν_4 resonance does not happen at all, while ν_3 and ν_5 are absent for about 0.1 Myrs from 0.4 to 0.5 Myr. Most of time, the resonant angles are smaller than 180° and the eccentricity stays low.

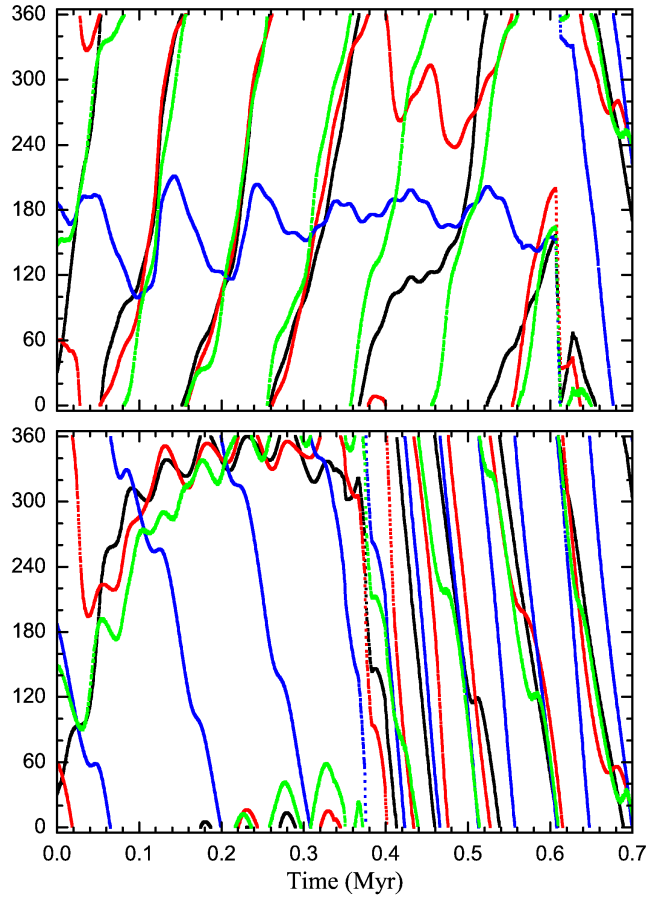


Fig. 15. The evolution of apsidal differences between the Trojans and the planets: $\Delta\varpi_2$ (black), $\Delta\varpi_3$ (red), $\Delta\varpi_4$ (blue) and $\Delta\varpi_5$ (green). The upper panel is for $i = 22°$ and the lower panel is for $i = 42°$.

The situation is quite different for $i = 22°$ (see Fig. 15, upper panel). The ν_4 resonance exists with the resonant angle around 180° all the way before the Trojan is expelled from the 1:1 MMR at $t \sim 0.63$ Myr. No other secular resonances are present until $t \sim 0.35$ Myr and the Trojan's eccentricity varies in correspondence with the circulation of the main secular angles $\Delta\varpi_k$ ($k = 2, 3, 5$). The critical eccentricity excitation happens when the ν_3 resonance sets in at $t \sim 0.35$ Myr. In this secular resonance the eccentricity reaches 0.25 at $t = 0.55$ Myr (red in Fig. 16), where the Trojan may approach to Venus closely. And this destabilizes the Trojan orbit.

For $i = 42°$ (see Fig. 15, lower panel) the resonant angles of ν_2, ν_3 and ν_5 librate around high values, resulting in a quick excitation of the Trojan's eccentricity to 0.45 (red in Fig. 16). Such a high eccentricity makes its orbit to cross the one of Venus, the one of Mars and finally the Trojan becomes unstable.

Based on these typical orbital evolutions we argue that the secular resonances $\nu_2, \nu_3, \nu_4, \nu_5$ are all involved in determining the Trojans' stability. Among them the ν_3 and ν_5 play more important roles than the others.

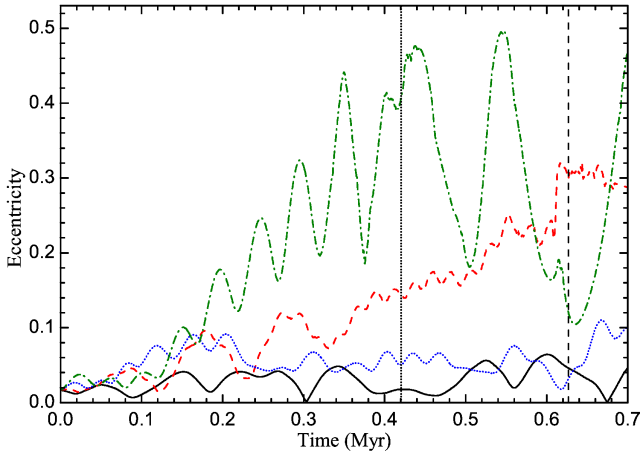


Fig. 16. The eccentricity evolution for four orbits. The solid curves represent the orbits with initial inclination $i = 10°$ (solid black), 22° (dash red), 35° (dot blue) and 42° (dash-dot green), respectively. The vertical dash and dot lines mark the moments when the orbits escape from the 1:1 MMR for $i = 22°$ and $i = 42°$, respectively.

5. Conclusions

We investigated in full detail the stability of the recently found Earth Trojan asteroid 2010 TK$_7$ in different dynamical models. We derived a symplectic mapping based on the spatial elliptic restricted three–body problem to see the location of the mean orbit in the context of the phase space structure. We tested the validity of the simplified model with numerical integrations and found good agreement of the model on short time scales. We included the influence of the additional planets as well as the Moon to see their influences on the mean orbit of 2010 TK$_7$. Next, we performed a detailed numerically study to propagate the orbit of the Trojan Earth asteroid both, forward and backwards in time together with 100 clone orbits to incorporate the possible errors of the orbital parameters induced by the observations. From the detailed study we are able to state the probability of capture and escape of the Earth Trojan together with the estimation of the time the asteroid will stay close to the Lagrangian point L_4 of the Earth. To this end we investigated in full detail not only the regime of parameters and initial conditions close to the actual found asteroid but rather on a grid of initial conditions and in the parameter space (a, i) using thousands of simulations, based on fictitious Earth-Trojans. With this we were able to define the region of stability and instability on both short and long time scales.

The main results of the present study can be summarized as follows: we can confirm the result of (Connors et al. 2011), the asteroid 2010 TK$_7$ lies in the tadpole regime of the Sun-Earth system. The orbital parameters indicate that most probably the asteroid became an L_4 Trojan some 1,800 years ago and it will jump to the L_5 neighbourhood or a horseshoe orbit in about 15,000 years in future. Before it moved to the current tadpole orbit this asteroid was captured into the 1:1 MMR around 30,000 years ago, and it may stay in the resonance for another 200,000 years. The total life-time of the asteroid (being in the 1:1 MMR) is less than 0.25 Myr. As a Near-Earth-

Asteroid, the closest approach of this asteroid to the Earth will be larger than 70 times the Earth-Moon distance when it is on a Trojan-like orbit. On short time scales it is possible to predict the orbit in the spatial elliptic restricted three-body problem (Sun-Earth-Asteroid) on intermediate time scales the influence of the Moon has to be taken into account. In addition, on longer time scales the influence of the other planets of our Solar system cannot be neglected, since the asteroid is on a chaotic orbit with close encounters to the unstable equilibrium L_3. We expect the discovery of further interesting objects in the vicinity of the L_4 or L_5 equilibria of the Sun-Earth system. The long term integrations show: for low inclinations the stability region extends in terms of semi-major axis up to $\pm.01$ AU. The size of it decreases with increasing inclination up to a threshold at about $i = 20°$. Another stability window opens up between 28° to 40° and disappears soon after. The preliminary results of our frequency analysis indicate that the ν_2, ν_3, ν_4 and ν_5 secular resonances are deeply involved in the motion of the Earth Trojans, and we show this by several examples.

From a qualitative point of view our simulations indicate that 2010 TK_7 is situated inside an unstable region where all sorts of orbits like horseshoes, tadpoles and jumping ones are possible. We show – this is well confirmed – the Earth Trojan moves on a temporary captured orbit. On the other hand it is unclear why there are no other Trojans of the Earth found up to now because there exist large stable regions for small inclinations, but also for larger inclinations Trojans may exist for very long time scales.

Acknowledgements. ZLY thanks the financial support by the National Natural Science Foundation of China (No. 10833001, 11073012, 11078001).

References

Bien, R., Schubart, J. 1984, Cel. Mech., **34**, 425
Bowell, E., Holt, H. E., Levy, D. H., Innanen, K. A., Mikkola, S., Shoemaker, E. M. 1990, BAAS, **22**, 1357
Brasser, R., Letho, H.J. 2002, MNRAS, **334**, 241
Brasser, R., Heggie, D., Mikkola, S. 2004, Celest. Mech. Dyn. Astron., **88**, 123
Breétagnon, P. 1974, A&A, **30**, 141
Chambers, J. 1999, MNRAS, **304**, 793
Connors, M., Wiegert, P., Veillet, C. 2011, Nature, **475**, 481
Delva, M., 1984, Celest. Mech. Dyn. Astron., **34**, 145
Dvorak, R., Schwarz, R. 2005, Celest. Mech. Dyn. Astron., **92**, 19
Dvorak, R., Schwarz, R., Süli, Á., Kotoulas, T. 2007, MNRAS, **382**, 1324
Dvorak, R., Bazsó, Á., Zhou, L.Y. 2010, Celest. Mech. Dyn. Astron., **107**, 51
Eggl, S., Dvorak, R. 2010, Lect.Notes Phys, **790**, 431
Érdi, B., Forgacs-Dajka, E., Nagy, I., Rajnai, R. 2009, Celest. Mech. Dyn. Astron., **104**, 145
Ferraz-Mello, S. 1997, Celest. Mech. Dyn. Astron., **65**, 421
Freistetter, F. 2006, A&A, **453**, 353
Hadjidemetriou, J. 1992, ZAMP, **37**, 776
Hadjidemetriou, J. 1999, Celest. Mech. Dyn. Astron., **73**, 65
Hadjidemetriou, J., Voyatzis, G. 2000, Celest. Mech. Dyn. Astron., **78**, 137
Hanslmeier, A., Dvorak, R. 1984, A&A, **132**, 203
Laskar J. 1999, Icarus **88**, 266
Lhotka, C., Efthymiopoulos C., Dvorak, R. 2008, MNRAS **384**, 1165
Lhotka, C. 2009, Celest. Mech. Dyn. Astron., **109**, 175
Li, J., Zhou, L.-Y., Sun Y.-S. 2006, Chin. J. Astron. Astrophys., **6**, 588
Lichtenegger, H. 1984, Celest. Mech. Dyn. Astron., **34**, 357
Mainzer, A., Bauer, J., Grav, T. and 32 coauthors 2011, ApJ, **731**, 53
Michtchenko, T.A., Ferraz-Mello, S. 2002 AJ **122**, 474
Mikkola, S., Innanen, K. 1992, AJ, **104**, 1641
Morais, M.H.M. 2001, A&A, **369**, 677
Morais, M.H.M., Morbidelli, A. 2002 Icarus **160**, 1
Morbidelli, A., Levison, H.F., Tsiganis, K., Gomes, R. 2005, Nature, **435**, 462
Murray, C.D., Dermott, S.F. 1999, Solar System Dynamics, Cambridge Univ. Press, Cambridge
Nesvorný, D., Vokrouhlický, D. 2009, AJ, **137**, 5003
Nesvorný, D., Thomas, F., Ferraz-Mello, S., Morbidelli, A. 2002, Celest. Mech. Dyn. Astron., **82**, 323
Nesvorn, D., Dones, L. 2002, Icarus, **160**, 271
Rabe, E. 1967, AJ, **72**, 10
Robutel, P., Gabern, F., Jorba, A. 2005, Celest. Mech. Dyn. Astron., **92**, 53
Robutel, P., Gabern, F. 2006, MNRAS372, 1463
Scholl, H., Marzari, F. 2004, Lunar and Planetary Science Conference **35**, 1107
Scholl, H., Marzari, F., Tricario, P. 2005, AJ **105**, 130
Schwarz, R., Gyergyovits, M., Dvorak, R. 2004, Celest. Mech. Dyn. Astron., **90**, 139
Schwarz, R., Dvorak, R. 2011, Celest. Mech. Dyn. Astron. (under review)
Tabachnik, S.A., Evans, N.W. 2000, MNRAS, **319**, 63
Tsiganis, K., Dvorak, R., Pilat-Lohinger, E. 2000, A&A, **354**, 1091
Wiegert, P. A., Innanen, K. A., Mikkola, S. 1997, Nature, **387**, 685
Zhang, S.-P., Innanen, K. A. 1995, AJ, **96**, 1995
Zhou, L.-Y., Dvorak, R., Sun, Y.S. 2009, MNRAS, **398**, 1217
Zhou, L.-Y., Dvorak, R., Sun, Y.S. 2011, MNRAS, **410**, 1849